

The effect of surface oxidation on the IASCC susceptibility of proton-irradiated type 316 stainless steel in hydrogenated PWR primary water

Yun Soo Lim*, Seong Sik Hwang, Dong Jin Kim, Min Jae Choi, Sung Hwan Cho
Nuclear Materials Safety Research Division/Korea Atomic Energy Research Institute
989-111 Daedeok-daero, Yuseong-gu, Daejeon 34057, Korea
*Corresponding author: yslim@kaeri.re.kr

1. Introduction

Irradiation-assisted stress corrosion cracking (IASCC) of austenitic 316 stainless steels, (SSs) commonly used in the internal components of a pressurized water reactor (PWR), is considered critical for safe long-term operation [1]. The IASCC mechanism is not fully understood, though it appears to be closely related to microstructural changes caused by neutron irradiation. The predominant failure mode of 316 SS in PWR primary water by IASCC is known to be intergranular, which means that the grain boundaries are the preferential paths for cracking. The surface oxidation phenomenon is thought to be a precursor of SCC because crack initiation can be triggered when a protective surface oxidation layer is ruptured by an applied stress. Proton irradiation is a useful experimental technique to study irradiation-induced phenomena in nuclear core materials instead of neutrons. Under the proper irradiation conditions, proton irradiation can produce a microstructure and microchemistry very similar to those by neutron irradiation [2]. The objectives of the present work were to investigate the surface oxidation and cracking behavior of a proton-irradiated type 316 SS specimens to obtain clear insight into the role of irradiation defects when this material is exposed to PWR primary water.

2. Methods and Results

2.1 Material and Proton Irradiation

Type 316 austenitic SS was used in this study. Its chemical composition is 16.14 Cr, 10.41 Ni, 0.047 C, 2.11 Mo, 1.08 Mn, 0.66 Si, 0.1 Al, 0.1 Cu, 0.003 P, and 0.001 S, with the balance being Fe (wt%). The test alloy was solution-annealed at 1100 °C and then quenched with water. Before proton irradiation, the surfaces of the specimens were electro-polished in a solution of 50 vol% phosphoric acid, 25 vol% sulfuric acid, and 25 vol% glycerol for 15 - 30 s at room temperature. Proton irradiation was performed with the General Ionex Tandatron accelerator at the Michigan Ion Beam Laboratory at the University of Michigan. The irradiation processes were conducted using 2.0 MeV protons at a current range of 40 μ A. The specimens were exposed at 360 °C to four levels of irradiation of 0.4,

1.6, 2.7, and 4.2 displacements per atom (dpa) at a depth of 10 μ m. The radiation damage levels of the samples were calculated with the Stopping and Range of Ions in Matter (SRIM) program using displacement energy of 40 eV in the 'quick calculation' mode.

2.2 SSRT and Surface Oxidation Tests

A slow strain rate test (SSRT) was conducted using flat tensile specimens to investigate the effects of the radiation dose of proton on the IASCC susceptibility of type 316 SS with a strain rate of 3.4×10^{-7} /s and total strain of 10 %. Coupons ($10 \times 10 \times 2$ mm³) for the surface oxidation test of the as-received and 2.7 dpa proton-irradiated type 316 SS were prepared by grinding with SiC paper to a 2000 mesh stage and subsequently polishing with alumina powders down to 0.3 μ m. The simulated PWR water was prepared prior to the test and held in a storage tank. In this study, 1200 ppm B (by weight) of H₃BO₃ and 2 ppm Li (by weight) of Li(OH) were added to pure water. The oxygen concentration was maintained at less than 5 ppb during the test. The test temperature was 325 °C with a dissolved hydrogen concentration of 25 cm³ H₂/kg H₂O. The oxidation coupons were exposed to the test solutions for a period of 5000 hrs.

2.3 Microstructural Analysis

Focused ion beam (FIB) TEM specimens from the test samples were prepared using a dual-beam Hitachi FIB-2100 system with Ga ions with an incident beam energy level of 30 kV and current of 1 – 5 nA. Final thinning was done at an acceleration voltage of 5 kV to eliminate the surface damage produced by highly energetic ions in the early stage of the FIB milling process. The test specimens were investigated using various types of microscopic equipment. A conventional TEM analysis of the crystallography and a compositional analysis of the oxidation layer was performed by energy dispersive X-ray spectroscopy (EDS) were conducted with a JEOL JEM-2100F device (operating voltage 200 kV).

2.4 TEM results of irradiation defects

It was found from the calculation using the SRIM program that the damage profiles of the type 316 SS

exhibited a slow increase roughly up to a depth of 15 μm as well as subsequent damage peaks near a depth of 20 μm from the irradiated surfaces when the acceleration energy of the protons was 2 MeV. In earlier work, it was revealed that the types of irradiation damage examined were point defects, dislocations and voids. Point defects and dislocations were found mainly in the area exposed to a low radiation dose; however, voids were dominant in areas exposed to a high radiation dose. More detailed information about the microstructural characteristics of proton-irradiated 316 SS is available in the literature [3].

2.5 Effects of proton irradiation on the surface oxidation behavior

The proton-irradiated specimens for the surface oxidation test were prepared such that the radiation dose on the surface was 4 dpa. The oxide morphologies on the surfaces of non-irradiated and proton-irradiated specimens are shown in Figs. 1(a) and (b), respectively.

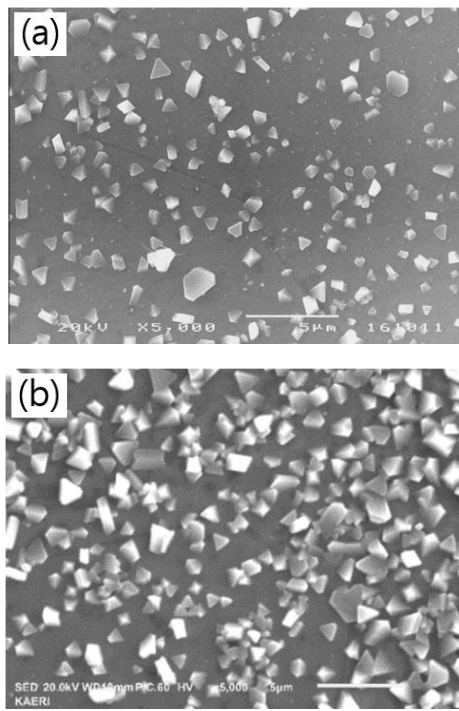


Fig. 1. SEM images of the surface oxide morphologies on a (a) non-irradiated matrix and a (b) proton-irradiated region with an average dose of 4 dpa of 316 stainless steel

The number density and the size of the surface oxides were increased for the proton-irradiated specimens compared to the non-irradiated specimens. It appears that the irradiation defects in the proton-irradiated specimen act as nucleation sites for oxides and promote the diffusion process of elements, resulting in rapid growth of the nucleated oxides. From the TEM/EDS measurements, the surface oxides in both specimens

were identified as Fe_3O_4 with very low concentrations of Si, Cr and Ni irrespective of proton irradiation.

Fig. 2(a) shows a STEM image of the surface oxidation layer around a grain boundary of the non-irradiated 316 stainless steel specimen and Fig. 2(b) shows the compositional variations of Cr, Fe and Ni obtained from line profiling EDS1 across a grain boundary just beneath the oxidation front denoted by EDS1 in Fig. 2(a). From Fig. 2(b), it can be confirmed that Cr/Fe levels were depleted and that Ni was enriched at the grain boundary. The as-received 316 SS showed no compositional changes across the grain boundary due to the solution-annealing treatment before the surface oxidation test. Therefore, it is evident that the compositional changes in Fig. 2(b) occurred during the process of surface oxidation. Oxygen diffuses into the matrix and reacts with less noble (more reactive) alloying elements such as Cr and Fe to form discrete oxides, leaving a Cr- and Fe-depleted grain boundary. Ni enrichment can be attributed to the fact that Ni, which is less active than Cr and Fe, was expelled to relieve the stress caused by the volumetric increase associated with the formation of the Cr and Fe oxides [4] and moved to the grain boundary.

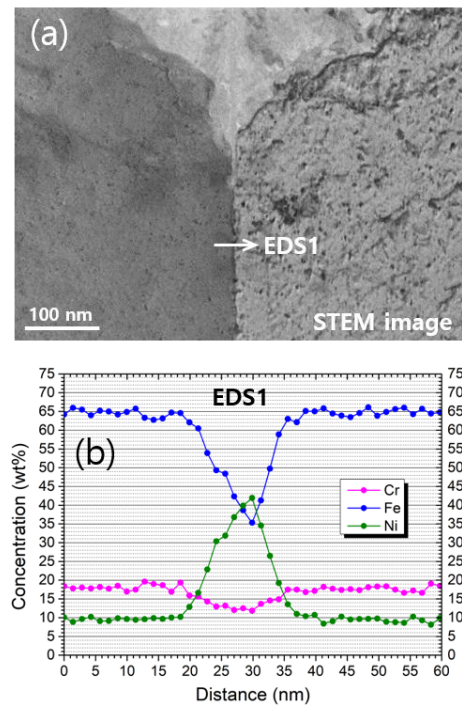


Fig. 2. (a) STEM image of the surface oxidation layer around a grain boundary of non-irradiated 316 stainless steel, and (b) compositional variations of Cr, Fe and Ni obtained from line profiling, as denoted by EDS1 in (a).

Fig. 3(a) shows a STEM image of the surface oxidation layer around a grain boundary of proton-irradiated 316 stainless steel and Fig. 3(b) shows the compositional variations of Cr, Fe and Ni obtained from the line profiling EDS2 across a grain boundary just

beneath the oxidation front denoted by EDS1 in Fig. 3(a). The phenomena of compositional changes, that is, Cr/Fe depletions and Ni enrichment, occurring at the grain boundary just below the oxidation front were basically identical to those in the non-irradiated specimen shown in Fig. 2. However, there is a remarkable difference in that the degrees of depletion and enrichment are much higher compared to those of the non-irradiated 316 SS. It is believed that the drastic changes in the chemical composition of the grain boundary in the proton-irradiated specimen were caused by the synergic effects of proton irradiation and surface oxidation.

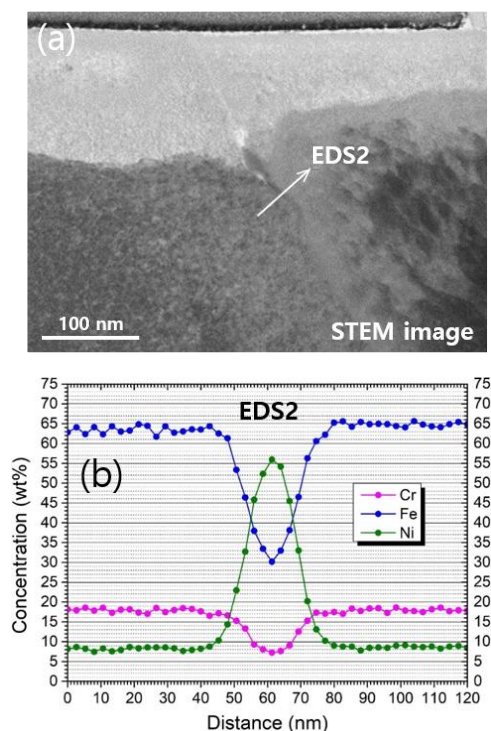


Fig. 3 (a) STEM image of the surface oxidation layer around a grain boundary of 4 dpa proton-irradiated 316 stainless steel, and (b) compositional variations of Cr, Fe and Ni obtained from line profiling, denoted by EDS2 in (a).

2.6 Influence of surface oxidation on the IASCC susceptibility

The characteristics of microstructural changes caused by irradiation and how they affect changes in the material behavior and IASCC have been extensively studied [5]. Irradiation of a material causes hardening, radiation-induced segregation and localized deformation. Uniform elongation is also reduced sharply when a material is irradiated. As such, the alloy becomes significantly embrittled in the PWR operation condition, which in turn makes it much more susceptible to IASCC by irradiation. Irradiation also affects the surface oxidation behavior in several ways. Irradiation defects such as vacancies and interstitials promote the diffusion

of alloying elements; therefore, more severe depletion of Cr and Fe along the grain boundaries occurs due to the synergic effect of radiation induced segregation (RIS) and surface oxidation (Fig. 3). Finally, the protective surface oxidation layer in the proton-irradiated 316 SS can fracture more easily through the greater accumulation of dislocations to the grain boundary compared to that of non-irradiated 316 SS when stress is applied [6].

All of these changes in the matrix and the surface oxidation behavior may increase the susceptibility to IASCC of proton-irradiated 316 SS. Much more research on surface oxidation phenomena appears to be necessary to obtain clear insight into the IASCC behavior of proton-irradiated 316 SS.

3. Conclusions

Type 316 SS was irradiated using 2 MeV protons with an average dose rate of $\sim 7.1 \times 10^{-6}$ dpa/s at 360 °C. Various irradiation defects, surface oxidation behaviors, and the degree of IASCC susceptibility induced by proton irradiation were characterized. The drastic changes in the chemical composition of the grain boundary in the proton-irradiated specimen were caused by the synergic effects of RIS and surface oxidation. The promotion of the diffusion of alloying elements by irradiation defects, the severe depletion of Cr along the grain boundaries by RIS and surface oxidation, and the easy rupture of the protective surface oxidation layers by grain boundary pile-up dislocations, including degradation of the mechanical properties, appear significantly to reduce the resistance to IASCC of austenitic 316 stainless steels installed near the core region of a PWR.

REFERENCES

- [1] J. McKinley, R. Lott, B. Hall and K. Kalchik, Examination of Baffle-Former Bolts from D.C. Cook Unit 2, Proc. of the 16th Int. Conf. on Environmental Degradation of Materials in Nuclear Power Systems-Water Reactor, 2013.
- [2] J. Gan and G.S. Was, Microstructure Evolution in Austenitic Fe-Cr-Ni Alloys Irradiated with Protons: Comparison with Neutron-Irradiated Microstructures, Journal of Nuclear Materials, Vol.297, p. 161, 2001.
- [3] Y.S. Lim, S.S. Hwang, D.J. Kim, M.J. Choi and J.Y. Lee, Microstructural Characterization of Proton-Irradiated Type 316 Stainless Steel, Trans. Kor. Nucl. Soc. Spring Meeting, Jeju Korea, May 23-24, 2019.
- [4] R.C. Newman and F. Scenini, Another way to think about the critical oxide volume fraction for the internal-to-external oxidation transition? Corrosion Vol.64 p. 721, 2008.
- [5] G.S. Was and S.M. Bruemmer, Effects of Irradiation on Intergranular Stress Corrosion Cracking, Journal of Nuclear Materials, Vol.216, p. 326, 1994.
- [6] T. Fujii, R. Yamakawa, K. Tohgo and Y. Shimamura, Analysis of the early stage of stress corrosion cracking in austenitic stainless steel by EBSD and XRD, Materials Characterization Vol.172, 110882, 2021